Supplementary information for

Promoter effects of alkali metal cations on the electrochemical reduction of carbon dioxide

Joaquin Resasco[1,2], Leanne D. Chen[3,4], Ezra Clark[1,2], Charlie Tsai[3,4], Christopher Hahn[3,4], Thomas F. Jaramillo[3,4] Karen Chan[3,4], and Alexis T. Bell[2,6,7]*

1. Department of Chemical Engineering, University of California, Berkeley, CA 94720

2. Joint Center for Artificial Photosynthesis, Material Science Division, Lawrence Berkeley National Laboratory, Berkeley, CA 94720

3. SUNCAT Center for Interface Science and Catalysis, Department of Chemical Engineering, Stanford University, Stanford, CA 94305

4. SUNCAT Center for Interface Science and Catalysis, SLAC National Accelerator Laboratory, Menlo Park, CA 94025

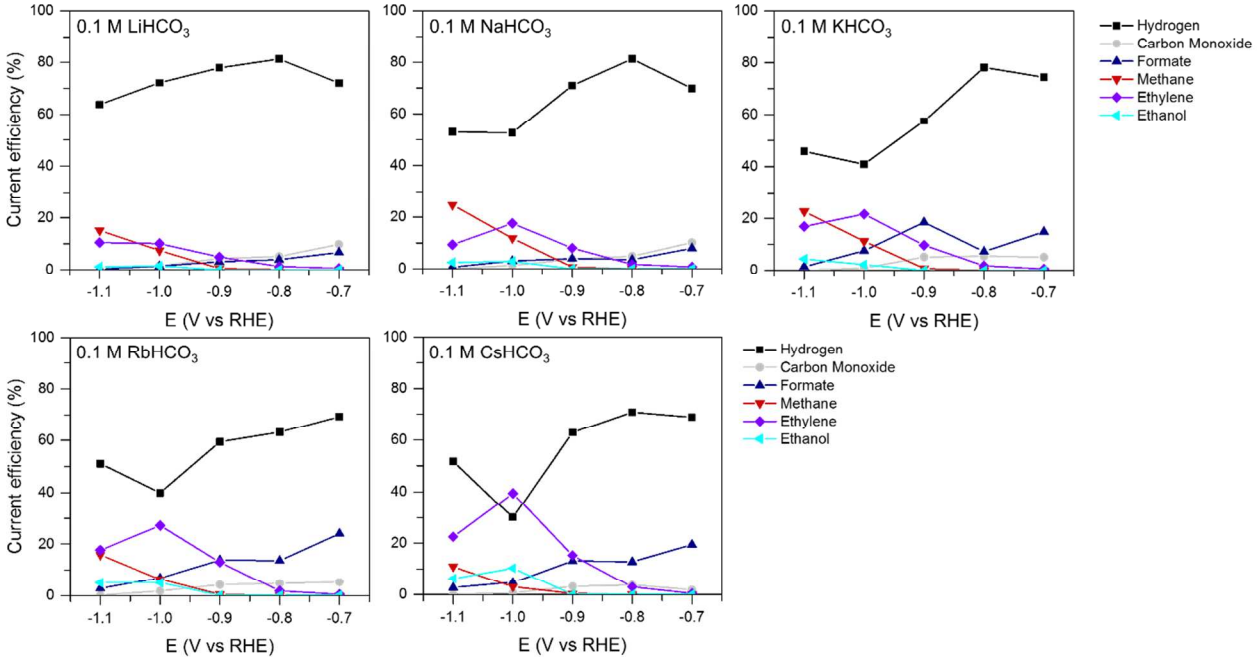

Figure S1: Product selectivities for electrochemical reduction of CO_2 on Cu (100). Faradaic efficiencies for the major products of CO_2 reduction on Cu (100) are shown as a function of the applied potential. Electrolysis is conducted in CO_2-saturated 0.1 M bicarbonate electrolytes containing different metal cations.

Figure S1 illustrates the faradaic efficiency of all major products (defined as those having a faradaic efficiency greater than 5%) as a function of the applied potential in CO_2-saturated bicarbonate solutions, each prepared with a different alkali metal cation. Selectivity and activity for minor liquid products can be found below (Table S1). The trends in product formation with increasing applied potential are consistent with those reported previously for K-based electrolytes,[1-2] and are qualitatively similar for all electrolytes compositions. At low overpotentials, CO_2 reduction is limited and hydrogen evolution dominates. Theoretical studies suggest that higher overpotentials are required in order to remove adsorbed hydroxyl species (OH*) from the surface of Cu and to reduce CO_2 to adsorbed carboxyl species (COOH*), the first intermediate formed.[3] At yet higher overpotentials, an increase in the Faradaic efficiencies to carbon monoxide and formate anions is observed. Finally, at the highest overpotentials, hydrocarbons and oxygenates begin to form as a consequence of the reduction of adsorbed carbon

monoxide.[4] The Faradaic efficiency to multicarbon products reaches a maximum near -1.0 V vs RHE.[1-2] At more negative potentials, concentration polarization become significant. This causes the pH near the surface of the catalyst to rise, which in turn results in a decrease in the local concentration of dissolved CO_2 due to the conversion of CO_2 to bicarbonate and carbonate cations. Under these circumstances mass transfer of CO_2 to the cathode through the mass transfer boundary layer becomes too slow to maintain the concentration of CO_2 near the electrode surface at its value in the bulk electrolyte.[5] At this point the total rate of CO_2 reduction is governed by the rate of CO_2 mass transfer through the hydrodynamic boundary layer rather than by the rate of reaction at the catalyst surface. The hydrogen evolution rate continues to increase for overpotentials lower than -1 V, resulting in an increase in the faradaic efficiencies for H_2 and the formation of methane, whereas the faradaic efficiencies for the formation of multicarbon products decrease. Figure S2 also shows that as the cation size increases for a fixed overpotential, the FE to hydrogen decreases, whereas the FEs to ethylene and ethanol is increase. However, since the overall current density also increases with cation size, product partial currents reflect more directly the activity shifts in the various products. For this reason partial currents, rather than faradaic efficiencies, are discussed in the main text.

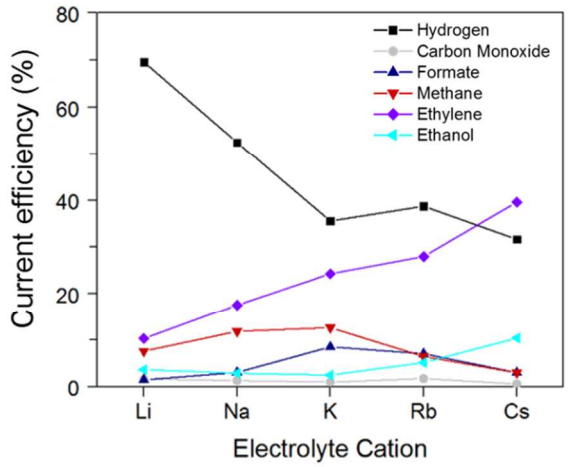

Figure S2: Product selectivities as a function of cation size for electrochemical reduction of CO_2 on Cu (100). Data is presented at -1.0 V vs RHE.

Table S1: Faradaic efficiencies (%) for minor liquid products for electrochemical reduction of CO_2 on Cu (100). Displayed at a potential of -1.0 V vs RHE

Product/ Cation	Li	Na	K	Rb	Cs
Glyoxal	0	0	0.10	0.13	0.11
Acetate	0	0	0.35	0.33	0.62
Glycolaldehyde	0	0	0.23	0.10	0.42
Acetaldehyde	0	0	0.63	1.05	0.83
Hydroxyacetone	0	0	0	0.13	0.11
Allyl Alcohol	0.39	0.33	1.89	2.01	1.19
Proprionaldehyde	0.88	0.82	1.48	1.18	0.96
Propanol	1.53	2.62	3.91	5.35	4.90
Total current	2.54	2.89	4.31	4.30	6.82

Table S2: Partial current densities (mA/cm^2) for minor liquid products for electrochemical reduction of CO_2 on Cu (100). Displayed at a potential of -1.0 V vs RHE

Product/ Cation	Li	Na	K	Rb	Cs
Glyoxal	0	0	4.30E-03	5.59E-03	6.82E-03
Acetate	0	0	1.51E-02	1.42E-02	4.23E-02
Glycolaldehyde	0	0	9.90E-03	4.30E-03	2.87E-02
Acetaldehyde	0	0	2.71E-02	4.52E-02	5.66E-02
Hydroxyacetone	0	0	0	5.59E-03	6.82E-03
Allyl Alcohol	9.89E-03	9.54E-03	8.14E-02	8.65E-02	8.19E-02
Proprionaldehyde	2.23E-02	2.37E-02	6.37E-02	5.08E-02	6.55E-02
Propanol	3.88E-02	7.57E-02	1.68E-01	2.30E-01	3.34E-01

Discussion on the effect of pH

Two competing effects must be considered to understand the result of increasing local pH on the final product distribution. At high pH, CO_2 will react with hydroxide ions to form bicarbonate, thus depleting the reactant, although this reaction is known to be slow.[6] Depletion of CO_2 will negatively affect the selectivity to CO_2 reduction products in general, and specifically on products containing more than one carbon. However, the formation of multicarbon products is proposed to proceed through a kinetically relevant carbon-carbon bond forming step that does not involve a proton/hydrogen transfer.[7-8]

This means that production of multicarbon products should be pH independent on an SHE scale, resulting in a higher relative rate to multicarbon products at high pH at a fixed potential on an RHE scale. This effect is responsible for the reduction in overpotential to form multicarbon products in alkaline solution in the reduction of carbon monoxide.[4] Whether the competing effects of CO_2 depletion or increased rates at high pH will be more significant, and therefore whether a high local pH will result in a higher rate to multicarbon products, depends on the extent of the local pH swing and the kinetics of the reaction between hydroxide in solution and CO_2. It is plausible then, that slight increases in local pH benefit selectivity to multicarbon products, while excessive polarization causes significant CO_2 depletion and a reduction in selectivity to multicarbon products.

Field effect on adsorbates without solvation

The pure field effect on various CO_2 adsorbates without ions or solvating waters was also investigated by applying a uniform field using a plain sawtooth potential, for fields in the range where the vacuum energy remains above the Fermi level. Figure S3 shows, as an example, the average potential profile along *z* for a field of 0.26V/Å applied using a sawtooth potential on adsorbed CH_3 on Cu (111). The right panels show top and side views of the atomic configurations.

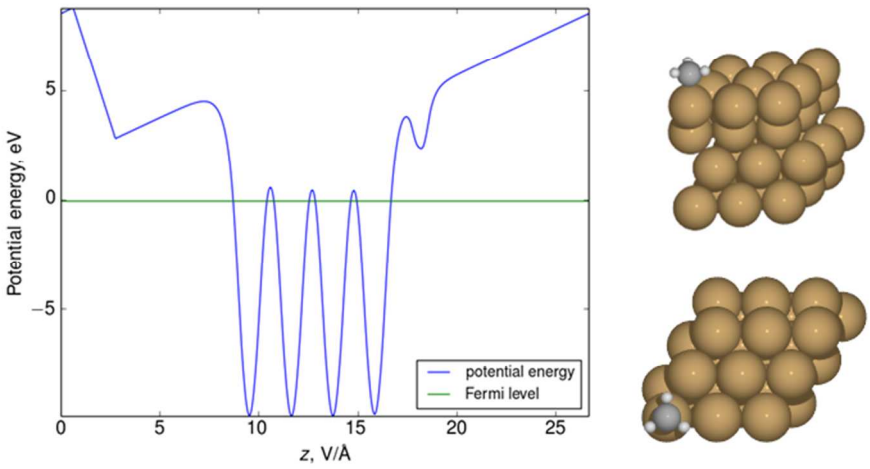

Figure S3. Left: Average potential energy along z with a field 0.26V/Å applied via a sawtooth potential for CH_3 adsorbed on Cu (111). **Right:** Side and top views of the corresponding structure.

Global optimization of solvation structures

An example of the full minima hopping optimization for solvated Li is shown in Fig. S4, where all new local minima found during the optimization are shown as successive steps. In panel B, only the new local minima that are found to be lower or equal in energy than all previous minima are shown. Figure S5 shows the solvation environment of each ion, with the Cu(111) surface removed for clarity. The solvation numbers are consistent with those recorded in literature.[9-10] The smaller cations from the series—Li^+ and Na^+— have a tighter solvation shell with 4 and 5 water molecules, respectively. This is consistent with solvation energies of cations increasing as cation size decreases.[11]

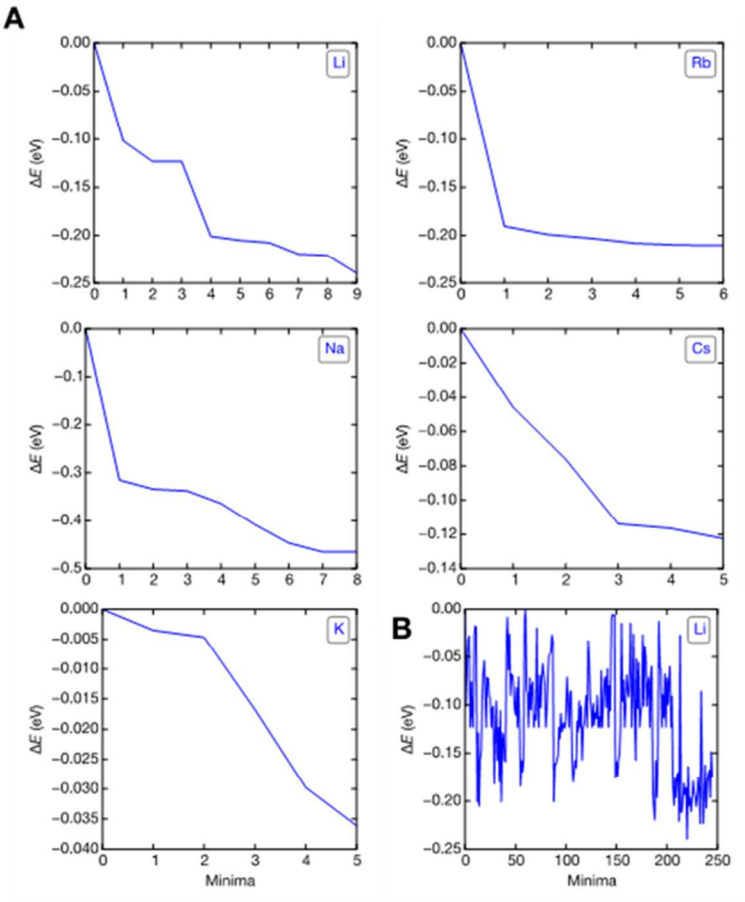

Figure S4: Global optimization of the water structures of solvated ions over a Cu (111) surface. a) all local minima found during the constrained minima hopping (CMH) global optimization that were lower or equal in energy to all previous local minima. B shows an example of a full CMH optimization for solvated Li, showing all local minima that were found, including those that were higher in energy than previous local minima. The plots shown in A are a subset of such minima searches, where only minima that are lower in energy are plotted.

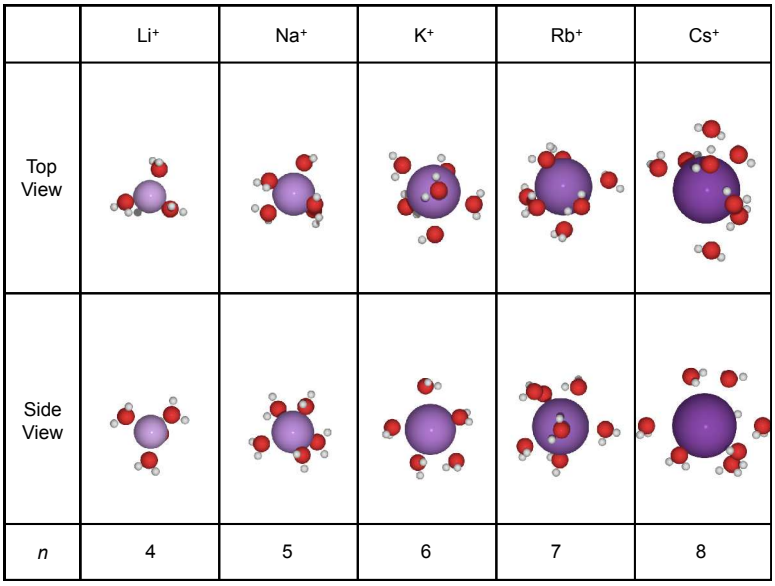

Figure S5. Local solvation structures around different alkali cations optimized via minima-hopping seen from two orthogonal planes. White spheres represent H atoms, red spheres represent O atoms, purple spheres represent various alkali cations, and *n* is the solvation number around each ion. The smaller cations (Li^+ and Na^+) have a tightly bound solvation shell, whereas the larger cations (K^+, Rb^+, and Cs^+) have a more loosely bound solvation shell comprising 6–8 water molecules.

Differences in field with cation size

Figure S5 shows the electric field distribution averaged over the center of the *CO adsorbate for each alkali cation. This electric field distribution was obtained via the following equation:

$$\mathcal{E} = \frac{\mathrm{d}\left(V_{\mathrm{env}} - V_{\mathrm{slab}} - V_{\mathrm{solvent}} - V_{\mathrm{ion}}\right)}{\mathrm{d}z}$$

where $\mathcal{E}$ represents electric field, V_{env}, V_{slab}, V_{solvent}, and V_{ion} are the electrostatic potential of the environment (without the adsorbate), the slab, the solvent, and the ion respectively. We note that the environment structures here show the metal Fermi level to lie at the edge of the solvent LUMO, which gives rise to some unphysical charge transfer from the metal to the water that doesn't occur in the structures that includes the adsorbate. This arises from the poor description of HOMO-LUMO gaps using

GGA-level functionals[12]. Further method development work is required to improve the accuracy of the field calculation.

Table S3 shows distance data for the optimized ion-slab distances on Cu(111), taken from the center of the alkali ion to the center of the Cu atoms in the 1st layer of the slab.

Table S3. Distance data optimized ion-slab distances

	Li^+	**Na^+**	**K^+**	**Rb^+**	**Cs^+**
Slab-ion distance	5.0Å	4.8Å	5.2Å	5.4Å	5.0 Å

Determination of ion energies

The energy of the alkali cation in bulk solution was referenced to the corresponding metal via the method developed by Nørskov et al. for proton-electron transfers[13]. Here we show a brief derivation of this principle taking Li as an example:

$$Li(H_2O)_4^+{}_{(aq)} + e^- \rightarrow Li_{(s)} + 4\ H_2O\ (l), \qquad U_0 = -3.04\ \text{V vs. SHE} \quad [2]$$

where the number of waters involved corresponds to the hydration number illustrated in Figure S5. At the equilibrium potential for this reaction, the free energy change is 0 by definition, and therefore we equate the chemical potentials of reactant and product:

$$\mu[Li(H_2O)_4^+] + \mu[e^-] = \mu[Li] + 4\ \mu[H_2O] \text{ at } -3.04\ \text{V vs. SHE} \quad [3]$$

To reference the energy of the lithium-electron pair to 0 V vs. SHE, we subtract 3.04 eV from the bulk metal (going toward a more oxidizing potential and therefore lowering the energy of the electron):

$$\mu[Li(H_2O)_4^+] + \mu[e^-] = \mu[Li] + 4\ \mu[H_2O] - 3.04\ \text{eV at } 0\ \text{V vs. SHE} \quad [4]$$

An ion solvated at the outer Helmholtz plane of an electrochemical interface has a partial electrostatic interaction with the surface, due to the overlap of solvent and slab charge densities. To probe the magnitude of this interaction, we compare the energy of the cation in bulk solution relative to that at the interface for each cation (again taking Li as an example):

$$Li(H_2O)_4^{+}{}_{(aq)} + e^- \rightarrow Li(H_2O)_4^{\delta+}{}_{(OHP)} + e^{\delta-} \quad [5]$$

The energy of the cation-electron pair, $Li(H_2O)_4^{\delta+}{}_{(OHP)} + e^{\delta-}$, is obtained explicitly through DFT calculations (similarly for the other cations) using the globally-optimized solvation structures placed at a fixed distance of 6.25 Å from the interface. The variation in with work function is determined using the charge-extrapolation scheme developed in Ref. [14-15]. Taking the previously obtained energy of the cation-electron pair $\mu[Li(H_2O)_4^+] + \mu[e^-]$, we can then obtain a driving force for Equation [5] for all cations.

References

1. Kuhl, K. P.; Cave, E. R.; Abram, D. N.; Jaramillo, T. F., *Energy Environ. Sci.* **2012,** *5,* 7050-7059.
2. Hori, Y.; Murata, A.; Takahashi, R., *J. Chem. Soc. Faraday Trans.* **1989,** *85*, 2309-2326.
3. Peterson, A. A.; Abild-Pedersen, F.; Studt, F.; Rossmeisl, J.; Norskov, J. K., *Energy Environ. Sci.* **2010,** *3*, 1311-1315.
4. Hori, Y.; Murata, A.; Yoshinami, Y., *J. Chem. Soc. Faraday Trans.* **1991,** *87*, 125-128.
5. Singh, M. R.; Clark, E. L.; Bell, A. T., *Phys. Chem. Chem. Phys.* **2015,** *17*, 18924-18936.
6. Pocker, Y.; Bjorkquist, D. W., *J. Am. Chem. Soc.* **1977,** *99*, 6537-6543.
7. Montoya, J. H.; Shi, C.; Chan, K.; Nørskov, J. K., *J. Phys. Chem. Lett.* **2015,** *6*, 2032-2037.
8. Goodpaster, J. D.; Bell, A. T.; Head-Gordon, M., *J. Phys. Chem. Lett.* **2016,** *7*, 1471-1477.
9. Mähler, J.; Persson, I., *Inorg. Chem.* **2012,** *51*, 425-438.
10. Varma, S.; Rempe, S. B., *Biophys. Chem.* **2006,** *124*, 192-199.
11. Burgess, J., In *Ions in Solution (Second Edition)*, Woodhead Publishing: 1999; 15-27.
12. Björketun, M. E.; Zeng, Z.; Ahmed, R.; Tripkovic, V.; Thygesen, K. S.; Rossmeisl, J., *Chem. Phys. Lett.* **2013,** *555*, 145-148.
13. Nørskov, J. K.; Rossmeisl, J.; Logadottir, A.; Lindqvist, L.; Kitchin, J. R.; Bligaard, T.; Jónsson, H., *J. Phys. Chem. B* **2004,** *108*, 17886-17892.
14. Chan, K.; Nørskov, J. K., *J. Phys. Chem. Lett.* **2015**, 2663-2668.
15. Chan, K.; Nørskov, J. K., *J. Phys. Chem. Lett.* **2016**, 1686-1690.